Journal of **Engineering Research**

TRANSIENT HEAT TRANSFER MODELING IN AN MFPL OPERATING IN BLOWDOWN MODE

Arthur Durigan Bahdur
``*Instituto Tecnológico de Aeronáutica*``, São José dos Campos, SP, Brazil
Master's student of the Space Science and Technologies course – PG/CTE.

Tiago Barbosa de Araújo
``*Instituto Tecnológico de Aeronáutica*``, São José dos Campos, SP, Brazil

Abstract: Modeling the heat exchange, in liquid propellant rocket engines (MFPL), between the gases resulting from combustion and the chamber walls, is essential to determine the type of material used in the chamber as well as its thickness, especially when there is no system of refrigeration. For MFPL's that operate in blowdown mode, this heat exchange is transient throughout engine operation, since there is no stationary mode of operation. The system used is based on an initial value problem of the engine's modus operandi, where the greatest pressure difference between the chamber and the propellant tanks is when the valves open, since the pressure in the chamber is ambient. To calculate the transient heat exchange, engine operating curves (pressure, thrust, mixture ratio, etc.) over time were first generated. With these, the convective and radiative heat exchanges between the gases and the chamber and the radiative heat exchange between the chamber and the external environment were calculated. The results showed that the greatest heat exchange is in the region close to the nozzle throat. Furthermore, for the engine analyzed, it was necessary to use a greater thickness in the nozzle region to avoid causing structural failure of the material.

Keywords: Rocket Engine, Liquid Propellant, Propulsion, Blowdown, Heat Exchange.

INTRODUCTION

The blowdown mode of operation of the MFPL (Figure 1), when it comes to hardware, is the simplest and least expensive. However, precisely due to its simplicity, this operating mode does not have control over the engine's operating parameters. Thus, its entire operation is in a transient regime, that is, all parameters vary over time: pressure in the tanks, pressure loss in the supply lines, pressure drop in the injector, mixing ratio, etc. MFPLs that operate for long periods typically have cooling systems, either by film cooling or by regenerative cooling via channels or perspiration, since no material is capable of resisting the temperatures that the chamber can reach (without being degraded/consumed) together with the pressure to which the engine is subjected (VASILIEV et al, 1993).

The present work is part of the development of a liquid propellant rocket engine with 90 N thrust at sea level, whose propellant pair is Hydrogen Peroxide 200 vol. (H_2O_2 50%) and Automotive Fuel Ethanol (ETOH 92.5%). The objective of this project is to be a low-cost and extremely simple MFPL in terms of hardware and operation, which is why such a propellant pair with blowdown operation was chosen. Figure 1 shows the simplified diagram of the MFPL power system.

Given the project objectives, the engine will not have a cooling system. Consequently, the analysis of the engine temperature at all points in the chamber, after and during operation, must guarantee, even without an active control system, that there will be no hot spots that could cause rupture and consequent structural failure.

There are 3 modes of heat transfer within the combustion chamber: convective, conductive and radiative. Convective heat comes from the flow of combustion gases inside the chamber; the conductive occurs on the walls of the combustion chamber and the radioactive is emitted by high temperature gases at the flame front. Figure 2 shows the analysis of convective heat using thermodynamic calculations in the boundary layer region.

The model used here to calculate the transient heat has as its main inputs the pressure and mixing ratio curve during blowdown operation, the modeling of which, including the injectors and the catalytic cradle, is beyond the scope of this article.
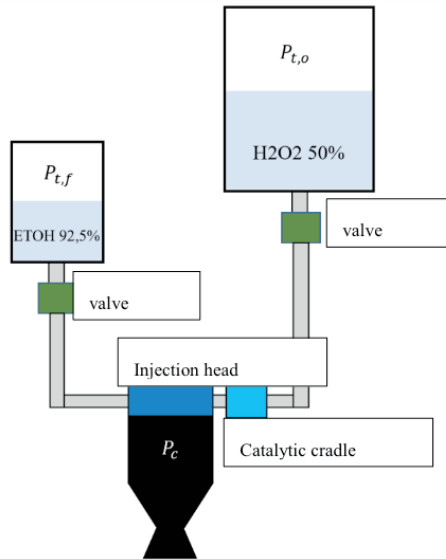
Figure 1. Simplified diagram of the MFPL power system
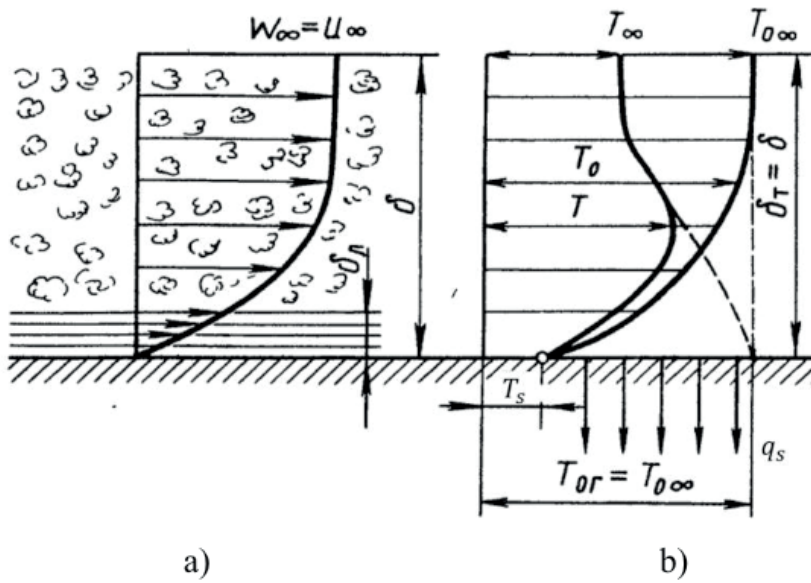
Figure 2. Illustration of boundary layers: a) dynamic CL – velocity gradient; b) CLT – temperature gradient. Adapted from (VASILIEV *et al*, 1993).

Since the pressure in the tanks is not constant – as propellant is consumed, the pressurizing gas is expanded and its pressure decreases – all other engine parameters change. The pressure in the tanks, chamber pressure, pressure drop in the injectors, propellant flow and pressure loss in the lines decrease, according to the qualitative graphs in Figure 3.

For the iterative combustion calculations, an interface in MatLab was used, made by the author, for the NASA CEA Software (GORDON; MCBRIDE, 1994), version of 2004. Its application at the project level was considered appropriate since it has wide validation in the American space program even without taking chemical kinetics into account, since the Software produces solutions in equilibrium or fixed composition (frozen). The results will be validated in the future with test bench testing.

METHODOLOGY

To calculate heat exchanges within the combustion chamber, adaptations of the methodology of Vasiliev et al (1993) were used, as it uses a stationary system. Some considerations are made for this first model:

- Conductive heat exchange on the combustion chamber wall is not considered, therefore an average wall temperature is adopted;

- For the calculation, the chamber is discretized into cross sections;

- Conductive heat exchange in the chamber wall in the longitudinal direction is not considered;

- The initial temperature of the chamber wall is the same as the environment, which is the same as that of the propellants in the tanks, adopted as 30º C;

- Variation in the mixing ratio throughout the combustion chamber is not considered, only in time;

- The combustion chamber material is 304 stainless steel;

- To reduce project costs, the engine nozzle will have a conical shape, with performance optimized for sea level (bench test site), in this version;

The chamber was divided into sections no longer than 1/20 of the chamber diameter and with refined division in the throat region where greater gradients are observed. Figure 4 exemplifies this idea. The constant time step chosen was 10 ms.

Therefore: $q^j_{c_i}$, $q^j_{rg_i}$, $q^j_{rc_i}$ e $T^j_{g_i}$, respectively, the convective, radiative heat fluxes between the gas and the wall, radiative between the wall and the external air, in section j and the temperature of the combustion gases in the iteration: i, and T_{amb} at room temperature, the total heat that passes through the chamber follows the methodology outlined in Figure 5. The calculation of each heat mode is done separately.

RADIATIVE HEAT FLOW BETWEEN COMBUSTION GASES AND THE CHAMBER

For this calculation, the mechanism hypothesis proposed in (BAHDUR, 2019), in appendix I, will be used. The maximum radiative heat flux is calculated according to equation 1.

$$q_{rg_i} = \varepsilon_{s,g}\sigma\left[\varepsilon_g T^4_{g_i} - \Lambda_g T^4_{s_i}\right] \qquad (1)$$

$$\varepsilon_{s,g} = \frac{\varepsilon_s}{1 - (1 - \Lambda_g)(1 - \varepsilon_s)} \qquad (2)$$

In the equation: 1, $\varepsilon_{s,g}$, ε_s, ε_g, Λ_g e σ are, respectively, the relative emissivity between the gas and the wall, the emissivity of the wall, the emissivity of the gas, the absorptivity of the gas and the Stefan-Boltzmann constant which is valid: σ=5,6697$x10^{-8}W/m^2K^4$.
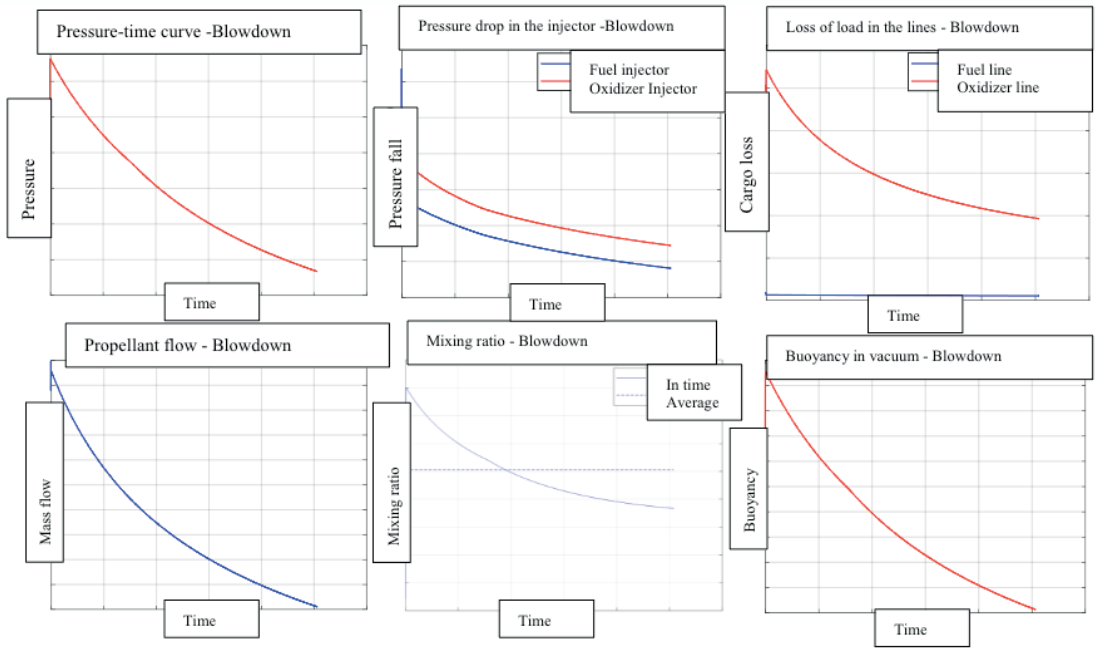
Figure 3. Characteristic graphics from the blowdown model.
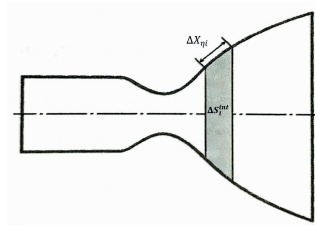
Figure 4. Division into chamber and nozzle sections. Adapted from (PEREIRA, 2010).
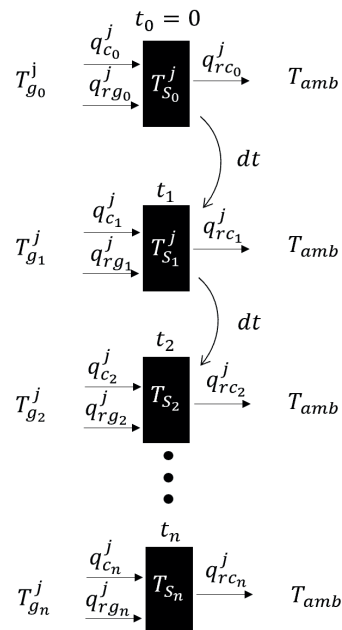
Figure 5. Heat exchange methodology in section j of the chamber wall over time.

In order to obtain a conservative result, some considerations are adopted:

- Complete combustion of the fuel;
- Non-dissociated gases.

To find the value of the radiative heat flow throughout the combustion chamber, the adapted methodology proposed by *Л. Ф. Фролов* (*L.F. Frolov*) which is shown by Vasiliev et al (1993), which consists of:

1. The radiative heat flux at the chamber entrance will be: $0{,}25q_{rg_i}$ and will increase logarithmically up to a distance of 50 mm from the entrance, reaching the value of q_{rg_i};

2. From the distance of 50 mm after the chamber inlet to the subcritical region (convergent of the nozzle), where the section diameter is: $1{,}2d_t$, the radiative heat flux will be: q_{rg_i};

3. From the previous point to the throat, the radiative heat flow will be: $q_{rg_i}[1-12{,}5(1{,}2-\bar{d}^2]$, $\bar{d}$ is the diameter of the section divided by the diameter of the throat: d_t;

4. In the throat the flow will be: $0{,}5q_{rg_i}$;

5. After the throat, in the supercritical region (supersonic – divergent), the radiative heat flux will be: $q_{rg_i}/2\bar{d}^2$.

RADIATIVE HEAT FLOW BETWEEN THE CHAMBER WALL AND THE ENVIRONMENT

The calculation of the radiative heat flow between the chamber wall and the environment is simpler and only depends on the temperature of the wall in section j, according to equation 3:

$$q_{rc_i}^j = \varepsilon_{s,ar}\varepsilon_s\sigma\left[T_{S_i}^{j\,4} - T_{amb}^4\right] \tag{3}$$

$$\varepsilon_{s,g} = \frac{\varepsilon_{ar}}{1-(1-\varepsilon_s)(1-\varepsilon_{ar})} \tag{4}$$

CONVECTIVE HEAT FLOW BETWEEN COMBUSTION GASES AND THE WALL

The calculation of the convective heat flow in each section, at each instant, was based on the methodology proposed by Vasiliev et al (1993). During the movement of gas within the combustion chamber, due to the high speeds, a turbulent zone is formed within the boundary layer. However, this region does not extend throughout it and, in the region closest to the wall, a laminar flow sublayer is formed. This type of flow has a peculiarity in which the exchange of heat through the surroundings occurs only through molecular processes (conduction and friction). Equation 5 governs the flow of heat exchange per unit area through the laminar region of the boundary layer considering these two effects:

$$q_c = -\left(\frac{k}{C_p}\frac{\partial H_p}{\partial y} + \mu_{visc}\frac{\partial u}{\partial y}u\right) \tag{5}$$

In which H_p is the enthalpy at the wall: μ_{visc} the viscosity of the flow, u the longitudinal speed, k, the thermal conductivity, C_p the average thermal capacity in the boundary layer and the variable: y represents the direction perpendicular to the chamber wall.

Therefore, $\frac{z_T}{z_\tau}$ is a ratio proportional to the conduction and friction heat exchange coefficients and $\beta_{r_i}^j$ the speed normalized by the maximum speed, the final equation governing the convective heat exchange in section j in the iteration: i is, according to equation 6:

$$q_{c_i}^j = B_i^j\frac{1-\beta_{r_i}^{j\,2}}{\bar{D}^{j\,1,82}}\frac{(p_{0c_i}\varepsilon_{0c_i})^{0,85}}{d_t^{0,15}}\frac{S_i^j}{Pr_i^{j\,0,58}} \tag{6}$$

$$S_i^j = \frac{(H_{p0r_i}^j - H_{ps_i}^j)\mu^{j\,0,15}_{visc_{1000,i}}}{R^{j\,0,425}_{0r_i}T^{j\,0,32}_{0r_i}\left(1+\bar{T}^j_{\,s_i}\right)^{0,595}\left(3+\bar{T}^j_{\,s_i}\right)^{0,15}} \tag{7}$$

$$B_i^j = \bar{a}_i\bar{A}_i^j(1000)^{-0,105} \tag{8}$$

$$\bar{a}_i = \frac{2^{1,18}}{4{,}42^{0,15}}\left(\frac{2}{\gamma_i+1}\right)^{\frac{0,85}{\gamma_i-1}}\left(\frac{2\gamma_i}{\gamma_i+1}\right)^{0,425} \tag{9}$$

$$\bar{A}_i^j = 0{,}01352 \left(\frac{z_T}{z_\tau}\right)_i^{j^{0,075}} \tag{10}$$

WALL TEMPERATURE INCREASE

The increase in temperature in the wall: $dT_{s_i}^j$, calculated as an average temperature in the area section: dS^j and mass dM^j, is then calculated using the total heat in the region, in the given time interval dt, according to equation 11:

$$dT_{s_i}^j = \frac{Q_{s_i}^j}{dM^j c_S} \tag{11}$$

$$Q_{s_i}^j = (q_{c_i}^j + q_{rg_i}^j - q_{rc_i}^j)dS^j dt \tag{12}$$

$$T_{s_{i+1}}^j = T_{s_i}^j + dT_{s_i}^j \tag{13}$$

RESULTS AND DISCUSSION

The graphs in Figures 6 and 7 represent the main results of the MFPL transient regime simulation. The variables: L_t and L_e represent, respectively, the location of the throat and the nozzle outlet.

Regarding the graph in Figure 6.a, the step in the final temperature curve (red) occurs in the region close to the engine convergent inlet (black line), which is where there is an increase in wall thickness, placed on purpose to reduce the final temperature of the material. The maximum temperature value obtained, close to the throat, was 1040 K, that is, around 767 ºC. This indicates that the engine will still operate in a safe range (for 304 stainless steel), according to working and melting temperature data (AISI, 1979).

Furthermore, the model used is conservative for the following reasons: Consideration of non-dissociated gases to calculate the gas stagnation temperature – as a result, the temperature becomes higher; Model without considering the evolution of conductive heat in the longitudinal direction of the chamber, this way all the heat is trapped in a small section. Even though this model is simplified, as the engine burns for a short period of time (less than 10 seconds), the conductive heat exchange will not be as intense, supported by the thermal inertia of the material; Furthermore, in order to confirm, in the simulations of Pagliuco (2003) it is shown that the Russian heat flow calculation model (similar to the one used here) promotes more conservative results than the American and French models.

As for heat flow (in the last iteration – Figure 6.b), as expected, the flow peak occurs in the region close to the throat. Furthermore, it is noted that the maximum radiative heat that the chamber emits into the environment occurs in the region of the wall's peak temperature. It is also worth mentioning that the main contribution to the increase in engine temperature is due to convective heat, which reaches (in this case) up to 20 times the radiative heat.

The graph in Figure 7 illustrates the different convective heat flow curves throughout the chamber at different moments of the burn. It is noted that there is an abrupt decrease in the heat flux that moves over time, in the upstream direction. After analyzing the discontinuity region using NASA CEA data, comparing all the parameters of the equations, the discontinuity was found in the wall enthalpy H_(ps_i) ^j. Analyzing the data shown in Figure 9, it is noted that the specific point is where liquid water condensation stops occurring. This point is known as Wilson Point, as shown by Young (1982) and Ding; Wang; Zhao (2014). It is also worth mentioning that after a certain moment of burning, the point ceases to exist and there is no more condensed water inside the chamber.

CONCLUSION

An iterative method for calculating the transient heat and thermal regime for an MFPL operating in blowdown mode was
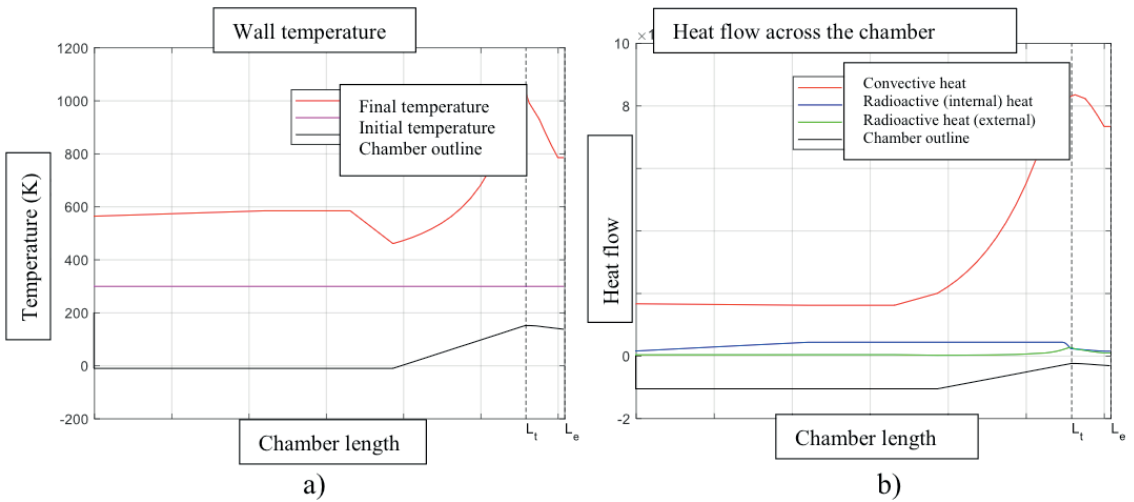
Figure 6. a)) Temperature values on the chamber wall at the beginning and end of the firing. b) Heat Flow throughout the chamber in the last iteration.

Figure graphics:
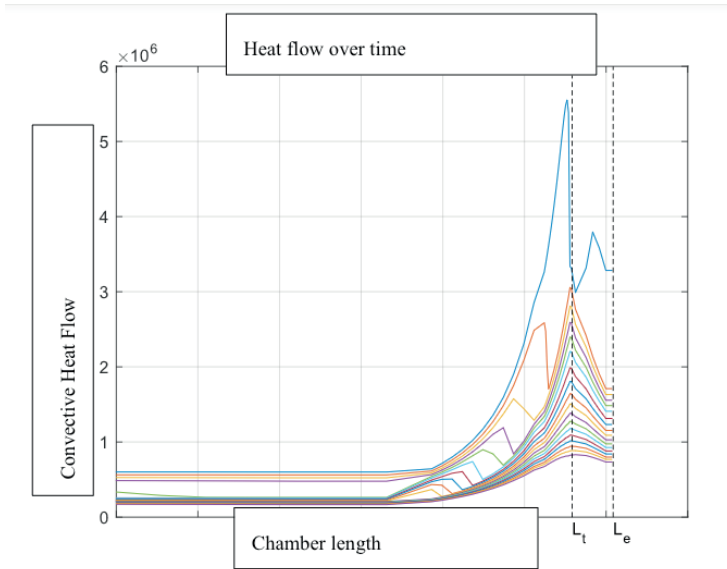
Figure 7. Heat Flow throughout the chamber in different iterations during firing.

MASS FRACTIONS	before			after
*CO2	0.17325	0.17325	0.17325	0.17325
H2O	0.23578	0.37292	0.37917	0.80357
*O2	0.02318	0.02318	0.02318	0.02318
H2O(L)	0.56779	0.43066	0.42440	0.00000

Figure 9. Simulation data between the points before and after the discontinuity.

proposed. The results obtained from the simulations indicate that the MFPL will work in a safe thermal region for 304 stainless steel, which will still be compared with data from test bench tests. The existence of Wilson Point was verified in the operation of this engine, since the percentage amount of water in the propellants (50% in the oxidizer and 7.5% in the fuel) is high. It is also worth mentioning that with the constant change in combustion and flow parameters during blowdown operation, the Wilson point also changes position in the upstream direction. The heat calculation model in the chamber can also be used in a steady-state system, such as engines pressurized by a gas tank or by turbopumps/ electric pumps. For simulations with longer burning times, a more accurate analysis of the conductive heat exchange in the longitudinal and radial direction of the combustion chamber is necessary, thus generating a two-dimensional model.

THANKS

REFERENCES

AISI. A Designer Handbooks Series 9004: High-temperature Characteristics of Stainless Steels. American Iron and Steel Institute, 1979.

BAHDUR, Arthur. Projeto de Câmara de Combustão de Motor Foguete à Propulsão Líquida de 25kN Pressurizado por Tanque. 2019. 272f. Trabalho de Conclusão de Curso. (Graduação em Engenharia Aeroespacial) – Instituto Tecnológico de Aeronáutica, São José dos Campos.

DING, Hongbing; WANG, Chao; ZHAO, Yakun. An analytical method for Wilson point in nozzle flow with homogeneous nucleating. International journal of heat and mass transfer, v. 73, p. 586-594, 2014.

GORDON, S., and MCBRIDE, B. J., "Computer Program for Calculation of Complex Chemical Equilibrium Compositions and Applications," NASA Ref. Publ. 1311, 1994.

PAGLIUCO, Cristiane Maria de Moraes. Projeto de Câmara de Empuxo de Foguete a Propelente Líquido. 2003. 90f. Trabalho de conclusão de curso (Graduação) – Instituto Tecnológico de Aeronáutica, São José dos Campos.

PEREIRA, Gabriel Costa Guerra. Projeto de Câmara de Combustão de Motor Foguete de 55kN a etanol e Oxigênio Líquido. 2010. 92f. Dissertação de Mestrado em Engenharia Aeronáutica e Mecânica – Instituto Tecnológico de Aeronáutica, São José dos Campos.

VASILIEV, A.P. *et al*. Fundamentos da Teoria e Cálculo de Motores Foguete a Propelente Líquido (*"Основы теории и расчета жидкостных ракетных двигателей"*). Moscou: Visshaia Schola, 1993. v. 1 e 2 (Originais em russo).

YOUNG, J. B. Spontaneous condensation of steam in supersonic nozzles. Physicochemical Hydrodynamics (PCH), v. 3, p. 57-82, 1982.